An examination of scaling behavior in unstable epitaxial mound growth via kinetic Monte Carlo simulations

IOP Publishing Journal of Physics: Condensed Matter
J. Phys.: Condens. Matter **31** (2019) 365301 (15pp) https://doi.org/10.1088/1361-648X/ab20b3

An examination of scaling behavior in unstable epitaxial mound growth via kinetic Monte Carlo simulations

Joshua P Schneider[1,2], Dionisios Margetis[3], Frederic Gibou[4] and Christian Ratsch[5,6]

[1] Department of Mathematics, University of California, Los Angeles, CA 90095, United States of America
[2] Department of Science, Technology and Mathematics, Gallaudet University, Washington, DC 20002, United States of America
[3] Department of Mathematics, and Institute for Physical Science and Technology, and Center for Scientific Computation and Mathematical Modeling, University of Maryland, College Park, MD 20742, United States of America
[4] Department of Mechanical Engineering and Department of Computer Science and Department of Mathematics, University of California, Santa Barbara, CA 93106, United States of America
[5] Department of Mathematics and Institute for Pure and Applied Mathematics, University of California, Los Angeles, CA 90095, United States of America

E-mail: cratsch@math.ucla.edu

Received 15 March 2019, revised 1 May 2019
Accepted for publication 9 May 2019
Published 28 June 2019

Abstract

We investigate the scaling behavior for roughening and coarsening of mounds during unstable epitaxial growth. By using kinetic Monte Carlo (KMC) simulations of two lattice-gas models of crystal surfaces, we find scaling exponents that characterize roughening and coarsening at long times. Our simulation data show that these exponents have a complicated dependence on key model parameters that describe a step edge barrier and downward transport mechanisms. This behavior has not been fully described in previous works. In particular, we find that these scaling exponents *vary continuously* with parameters controlling the surface current. The kinetic processes of the KMC models that we employ include surface diffusion, edge diffusion, step-edge barriers, and also account for transient kinetics during deposition via *downward funneling* and *transient mobility*. Our extensive simulations make evident the salient interplay between step-edge barrier strength and transient kinetic processes.

Keywords: epitaxial growth, mound formation, KMC simulations, thin films, surfaces, nano structures

(Some figures may appear in colour only in the online journal)

1. Introduction

Epitaxial growth has been extensively studied both experimentally and theoretically, as a subject of technological importance and fundamental scientific interest. However, far-from-equilibrium material systems often exhibit unanticipated behavior. Even in the relatively simple setting of homoepitaxial growth, the microscopic origin of complex phenomenology may take decades to fully understand. Consider, for example, the re-entrant 'smooth' growth observed in metal-on-metal epitaxy [1, 2]: it took nearly twenty years to discern the roles of the several atomistic mechanisms contributing to the non-intuitive low-temperature behavior of such a simple system [3]. Discoveries of this kind have been largely enabled by improved simulations of crystal systems, which are aided in part by advances in computer hardware and algorithms.

[6] Author to whom any correspondence should be addressed.

An aspect of homoepitaxy for which modern simulation capabilities may be crucial is the evolution of mounds during unstable growth. In this paper, we reexamine fundamental aspects of homoepitaxial growth by carrying out extensive atomistic simulations. We find that scaling exponents characterizing unstable growth of mounds at long times have a complicated, previously unnoticed dependence on physical parameters that are intimately linked to key atomistic processes.

In contrast to heteroepitaxial mounding, which has a thermodynamic origin, many high-symmetry crystal surfaces admit a kinetically-induced mounding instability during growth [4]. Specifically, the Ehrlich–Schwoebel (ES) step-edge barrier to interlayer diffusion [5, 6] promotes a destabilizing *uphill surface current* in the presence of external material deposition, leading to mound formation and steepening (see figure 1). After several monolayers of material deposition, however, the average mound slope tends to saturate [2, 7–10], a phenomenon that is known as *slope selection*. To explain the apparent stabilization of mound slope in experiments, two transient processes have been proposed as the primary mechanisms: *downward funneling* (DF) [2, 11–13] and *transient mobility* (TM) [11, 14–16]. In both DF and TM, freshly deposited atoms quickly relax to energetically favorable positions near deposition sites, albeit in slightly different ways: DF is characterized by downward transport of deposited atoms, whereas TM may also involve significant lateral transport. The net effect in both cases is a slope-dependent, *downhill current* that competes with the ES-barrier-induced uphill current. Without these downward transport mechanisms, the step-edge barrier would lead to slopes that increase indefinitely as the mounds grow.

Our goal with the present work is to show that the scaling behavior of homoepitaxially grown mounds in the presence of DF and TM is more complicated than previously thought. In particular, we illustrate the influence on related scaling exponents of a variety of kinetic processes such as ES barrier, step-edge diffusion, and transient processes associated with material deposition that contribute to a downhill current on simple cubic (SC) and body-centered cubic (BCC) crystal surfaces. To this end, we obtain and analyze a much more comprehensive data set than what has previously been available.

For given coverage, θ, useful statistical characterizations of homoepitaxial growth of mounds include the surface roughness (root mean square deviation in surface height), $w(\theta)$, and the lateral mound size, $r_c(\theta)$. For large enough coverage, $\theta \gg 1$, these quantities are generally expected to follow power laws of the form

$$w \sim \theta^{\beta} \tag{1a}$$

and

$$r_c \sim \theta^{n}, \tag{1b}$$

where β denotes the roughening exponent and n is the coarsening exponent. The symbol $\sim$ expresses proportionality for high enough θ by omission of the related constant prefactor on the right-hand side. By equation (1), the average mound slope can be estimated by the ratio w/r_c. Therefore, slope selection occurs when $\beta - n$ becomes negligible. The existence of stable slopes and the precise nature of growth laws (1) depend on the conditions of growth, and can be sensitive to atomistic kinetic processes related to deposition and surface diffusion. For general reviews on this subject, see, e.g. [17, 18].

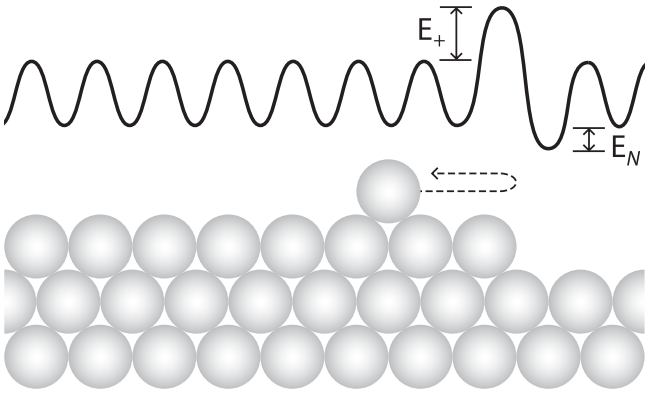

Figure 1. Illustration of the effect of the ES step-edge barrier (side view). An adatom diffusing toward a descending step edge must overcome an additional energy barrier, E_+, in order to attach to the step. Larger barriers increase the probability that an adatom is reflected toward the center of the terrace.

Exponents β and n have been studied previously by many researchers via analytical tools [19–31], computer simulations [3, 12, 13, 16, 32–39], and laboratory experiments [2, 7–10, 40–42] (see section 2). We note in particular that Stroscio *et al* measured $n = 0.16$ for Fe/Fe(0 0 1), and that Zuo and Wendelken measured $n = 0.25$ for Cu/Cu(0 0 1).

The results of our atomistic simulations indicate that these past studies are not definitive. Most notably, we find that the scaling exponents β and n vary continuously as a function of the model parameters related to atomistic processes that influence the mass current on a growing crystal surface. It is worthwhile to note that, in comparison to results presented, e.g. in [12, 33], our results here include more values for the step-edge barrier; and we also employ two transport mechanisms in the form of DF as well as TM. The latter improvement allows us to explore roughening and coarsening *as a function of downward transport strength* (which can be varied by varying the size of the TM search area; see section 3.3), which is not addressed in [12, 33]. Furthermore, our simulations account for a larger number of monolayers of deposition for all cases, in comparison to previous studies [12, 16, 33–35, 38, 39]. Leveraging this newly obtained, extensive data, more accurately computed coarsening exponents, and over a decade of additional literature, we can now re-examine some of the issues related to observations of earlier studies [8, 12, 16], as explained in section 2.

At this point, it is useful to make a distinction between the 'asymptotic' behavior of unstable growth, in which scaling exponents of interest approach universal values for very large coverage, from 'long-time' behavior. At long times, exponents measured from data may differ from asymptotic values, but show little variation as time increases. This long-time but not asymptotic behavior is often appropriately referred to as the 'transient regime', and extracted exponents are called effective scaling exponents. The asymptotic regime is not always practically attainable via atomistic simulations. However, slope selection ($\beta \approx n$) is a good indication that asymptotic values

of exponents have been obtained. Traditionally, an appealing means of determining the asymptotic (in time or coverage) values of exponents β and n in equation (1) has been the analysis of continuum models for crystal surfaces (see, e.g. [19, 24, 37]). This approach deserves particular attention, and has stimulated a plethora of studies. However, results of this approach may be deemed as questionable or incomplete since they are usually derived from phenomenology, with no direct connection to the key atomistic processes underlying epitaxial growth. At the same time, while experimental observations of the growth process are the preferred source of information about power laws such as equation (1), the corresponding available data sets are limited. In light of these considerations, atomistic simulations capturing *long-time behavior* appear as a promising and viable alternative in cases where the asymptotic regime is out of reach.

In this paper, motivated by the need for more accurate and physically reliable computations of epitaxial growth, we present *extensive* kinetic Monte Carlo (KMC) simulation results that study in detail the effect of different kinetic processes. For example, our computations include more than three dozen parameter sets, each of which involve several ensembles of simulated growth of 1000 monolayers of deposition on lattices of size 1000×1000, where we use dimensionless parameters and, thus, set the lattice constant, a, equal to unity ($a = 1$). All simulations start with an initially perfectly flat surface (so that they always have the same initial conditions). These simulations have enabled us to generate a data set that is much more comprehensive than the data previously available. The interpretation of these results suggests new physical insights into unstable epitaxial growth, as we discuss below.

The remainder of the paper can be outlined as follows. Section 2 provides a review of previous works related to the scaling behavior of unstable epitaxial growth and further motivates our present study. In section 3, we describe the lattice-gas models that we employ in our KMC simulations including the basic solid-on-solid (SOS) model (section 3.1) and effect of ES barrier (section 3.2); and give details of the downward transport mechanisms DF (section 3.4) and TM (section 3.3). In section 4, we discuss *qualitative* features of mound morphology as a function of model parameters. In section 5, we *quantitatively* characterize different mounding scenarios, highlighting the dependence of roughening and coarsening exponents on the KMC model parameters. Finally, section 6 concludes our work with a summary of our findings and an outline of open problems.

2. Past works and motivation

In this section, we review previous theoretical research on the scaling laws for roughening and coarsening during unstable homoepitaxial mound growth. This research includes both atomistic and continuum approaches. We also make an effort to place our findings in the context of these past works. Comprehensive reviews of a large part of the literature discussed here can be found in [17, 18].

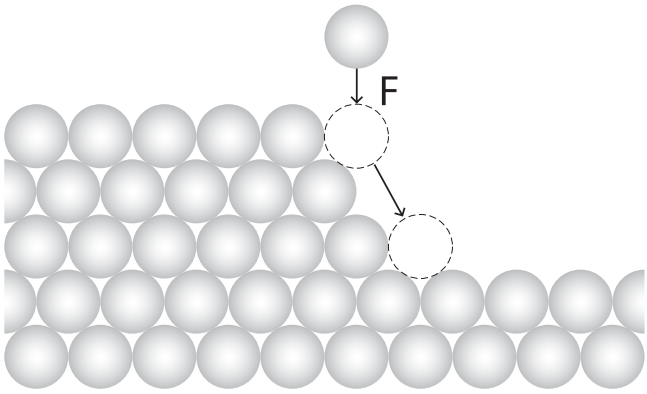

Figure 2. Illustration of the basic DF mechanism (side view) [2], where freshly deposited atoms (rate F) relax to an adsorption site with the maximum number of neighbors in the layer below.

2.1. Simulations of atomistic models

Next, we focus on theoretical approaches that rely on simulations of key atomistic processes of epitaxial growth. To the best of our knowledge, Evans and coauthors are the first to suggest DF as a mechanism contributing to slope selection, and explore its consequences during growth [2, 11, 13, 34]. Their initial model of DF, which we employ in our own KMC simulations (figure 2), involves the descent of newly deposited atoms down to a site with 'full support', namely, the maximum number of neighbors in the next lower layer [2, 34]. A refinement of the original DF model, termed restricted DF, is introduced in [13] in order to more accurately capture low temperature deposition dynamics; in this version of DF, atoms do not necessarily descend to a site with full support.

In a similar vein as Evans [2], Šmilauer and Vvedensky show that slope selection is also a feature of an atomistic model including TM [15, 16]. In [16], the authors point out that selected slopes result from a competition between: (i) roughening, which increases the average slope; and (ii) coarsening, which decreases the slopes. Roughening is primarily influenced by the strength of the ES barrier, whereas coarsening is a result of mechanisms that fill in valleys between mounds; e.g. detachment of atoms from edges of steps or downward transport.

The TM scheme employed by Šmilauer and Vvedensky is one of only a few descriptions for transient diffusion of adatoms, or 'hot precursors', suitable for incorporation in KMC simulations [15, 16]. For this reason, we make use of their algorithm, described in [16], for KMC simulations involving TM (figure 3). As detailed in sections 3–5, we thoroughly portray the consequences of this TM scheme by expanding available parameter sets of simulations, especially the range of ES barriers and 'search radius', R, i.e. the length scale for transient diffusion. Our results confirm that slope selection occurs in simulations including both ES barriers and TM. However, additional findings in our simulations may suggest differences from the results in [16]. For instance, in the case of variable ES barriers, the authors in [16] claim that increasing the barrier strength decreases the coarsening

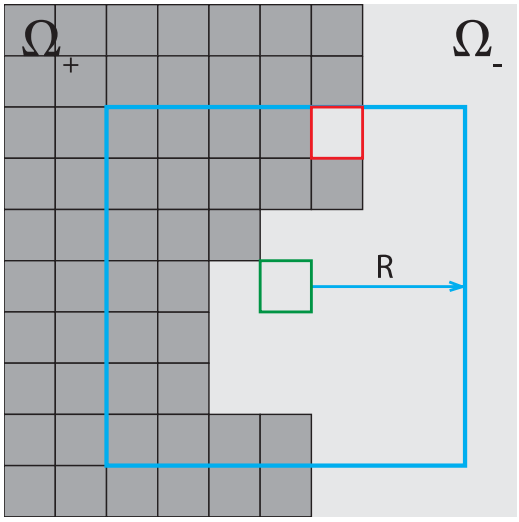

Figure 3. Illustration of the KMC prescription of TM, where freshly deposited atoms relax to a nearby site with highest coordination (top view). The site shown in green is the lattice site initially chosen for deposition, the square in blue contains the sites explored during TM, *R* defines the square where the search is performed, and the site shown in red is the final destination of the deposited atom after it has thermalized.

rate. In fact, we observe the *opposite* effect: larger barriers may lead to larger coarsening exponents. Furthermore, as *R* increases, we observe a continuous change of the scaling exponent describing surface slope, which contrasts the suggestion put forth in [16] that slopes remain constant for large enough *R*.

We should also highlight results in atomistic simulations of unstable epitaxial growth of mounds obtained by Amar and coauthors [3, 12, 33, 39, 43–45]. In [12], Amar and Family use KMC simulations with DF to study the roughening and coarsening of mounds, extending their previous results by considering a range of different ES barriers and deposition rates in their parameters. The coarsening rates for mounds computed in [12] are different in the respective regimes of small and large ES barriers. The authors in [12] conclude that: either (i) the combined cases with small and moderate barriers have an extended transient regime compared to the case with a large barrier; or (ii) there is a transition from an asymptotic coarsening rate to another based on a competition between kinetic processes influencing the coarsening of mounds. One such kinetic process is step-edge diffusion, i.e. the transport along a step edge of atoms with only a few in-plane near neighbors. This process is the primary focus of a follow-up paper by Amar [33]. In this work [33], the author concludes that the kink-Ehrlich–Schwoebel barrier can significantly impact the coarsening rate of mounds. Specifically, the incorporation of an infinite barrier of this type into the simulations leads to a slower coarsening compared to the case without such a barrier, for both (0 0 1) and (1 1 1) surfaces.

At the risk of redundancy, we repeat that, in contrast to the results presented in [12, 33], our findings rely on five values for the step-edge barrier. In addition, we invoke two transport mechanisms in the form of DF as well as TM. Because of this latter improvement, we are able to explore roughening and coarsening *as a function of transport strength*, which is not addressed in [12, 33]. Furthermore, our simulation data account for 1000 monolayers of deposition for all cases, whereas previous simulation data only account for approximately 400 monolayers [12, 33]. Consequently, we believe that we can make more detailed observations related to transient versus asymptotic roughening and coarsening behavior in epitaxial systems (see sections 4 and 5).

2.2. Analysis and simulations of continuum models

Another approach to unstable homoepitaxial growth of mounds relies on the analysis or simulation of phenomenological continuum models of crystal surfaces [19–27, 29–31]. This type of study invokes a family of partial differential equations (PDEs) by which the surface height profile in crystal growth becomes unstable toward mounding. This instability, which may result from the presence of ES barriers at step edges [4], enters the continuum evolution equations through one of two plausible types of slope-dependent surface mass current. Specifically, the surface current either (a) promotes the continuous steepening of mounds, or (b) leads to slope selection.

In particular, Sander and coauthors are apparently the first researchers to study each type of surface current [7, 8]. The work reported in [8], which includes modeling and simulation of crystal surfaces with slope selection, mainly focuses on a 6th-order PDE, which is distinct from the more frequently used 4th-order evolution equations based on the use of the capillary term of surface diffusion by Mullins [46]. In their corresponding continuum model [8], these authors provide an argument for the possible exclusion of the 4th-order term on the basis that the system under investigation, namely, Fe on F(0 0 1) at room temperature, is irreversible. Numerical simulations then reveal a coarsening exponent $n \simeq 1/6$ in this case [8]. Furthermore, in [8] the authors replace the 6th-order term in their simulated PDE with a 4th-order capillary term, and find that coarsening obeys a power law with $n \simeq 1/4$. This result suggests that there is a crossover of the coarsening exponent depending on the relative importance of the 4th-order and 6th-order terms in the PDE for the crystal surface height.

Our simulation results corroborate this speculation. We are tempted to entertain the scenario that under certain growth conditions both 4th-order and 6th-order terms are present in the appropriate continuum limit of the atomistic model. Furthermore, the step edge barrier may control the relative importance of each term, thus causing a continuous transition of the coarsening exponent, n, from 1/6 to 1/4. Our conclusions are discussed in section 6.

Another noteworthy research effort, led by Siegert *et al* [19, 21, 22, 37], focuses on the analytical and numerical investigation of PDEs with and without slope selection. By drawing an analogy with the coarsening dynamics encountered in phase ordering, which has been successfully described by Bray's theory [47], these authors [19, 21] show that mounds, with typical size $r_c(\theta)$, should coarsen with time (or, coverage θ) according to equation (1*b*) with $n = 1/3$. This

exponent amounts to the Lifshitz–Slyozov–Wagner law [48, 49]. However, this result [19, 21] contradicts experimental and numerical evidence, including simulations in [7, 8, 20], which have suggested that $n \simeq 1/4$. Later, Siegert discovers that his application of Bray's theory [47], which presumes the existence of only one relevant length scale, is incorrect [37]. Specifically, in [37] the author points out that *two* length scales emerge in scenarios that admit square mounds: in addition to the typical mound size, r_c, a second, long length scale describes the average spacing between occasional *dislocations* (defects) in the superlattice formed by square mounds. These features do not neccessarily coarsen at the same rate. Before the appearance of this work [37], the assumption of a single length scale had not been questioned. In light of this discovery, coarsening exponents reported in earlier works should be interpreted with caution: it is possible that these works measure a combination of mound *and* dislocation coarsening rates instead of a rate pertaining exclusively to the coarsening of mounds.

Following the aforementioned breakthrough regarding the existence of two scales for mounds with square symmetry, Golubović *et al* [25, 27, 50] confirmed that coarsening exponents depend on the crystalline symmetry. In these works, extensive simulations of PDE models with slope selection show that $n \simeq 1/4$ in cases with square symmetry, whereas $n \simeq 1/3$ for isotropic or hexagonal symmetry, independent of step-edge barrier strength. In [25], the authors argue that certain slope–slope correlation functions can be used to accurately these correlation functions, which we employ in our our statistical characterization of mound morphologies (section 2.3), can be found in section 5.

We should add a few more remarks on the relation of our work to the analytical and numerical studies performed on phenomenological continuum models, particularly [25, 37]. In these works, the authors attempt to obtain asymptotic values of scaling exponents for roughening and coarsening, which are not always practically attainable via atomistic simulations. Instead, our results pertain to long times, i.e. for up to 1000 monolayers of deposition, which in cases without slope selection yield *effective scaling exponents* instead of asymptotic values. In spite of this difference in predictions, we are still able to apply the physical principles illustrated by continuum treatments: for example, our results are consistent with: (i) the realization of Siegert *et al* [37] that multiple long length scales should be accounted for when assessing the coarsening rate of square mounds; and (ii) the property that scaling exponents may be affected by the choice of reversible or irreversible growth (see [8] where the 4th-order versus 6th-order terms in PDEs for surface height are discussed).

2.3. Revisiting correlation functions

In this subsection, we revisit three kinds of correlation functions that we employ in our statistical characterization of surface morphologies. We also explain how these functions are used to determine scaling exponents for roughening and coarsening.

The statistics of surface profiles obtained in KMC simulations are most conveniently expressed via the height–height correlation function, $G_{\mathrm{hh}}(r,\theta)$, and two slope–slope correlation functions, namely, the *longitudinal* slope–slope correlation function, $G_{\mathrm{lss}}(r,\theta)$, and the *transverse* slope–slope correlation function, $G_{\mathrm{tss}}(r,\theta)$. Here, $r = |\mathbf{r}|$ is the polar distance where $\mathbf{r}$ denotes the position vector in the high-symmetry plane of the crystal. Let $h(\mathbf{r},\theta)$ denote the surface height as a function of position, $\mathbf{r}$, and coverage, θ. The height–height correlation function is defined as

$$G_{\mathrm{hh}}(r,\theta) = \langle \tilde{h}(\mathbf{r},\theta)\tilde{\mathbf{h}}(\mathbf{0},\theta)\rangle, \tag{2}$$

where $\tilde{h}(\mathbf{r},\theta) = \mathbf{h}(\mathbf{r},\theta) - \langle \mathbf{h}(\mathbf{r},\theta)\rangle$ and $\langle\cdot\rangle$ denotes the average computed via a choice of the origin of the coordinate system and ensembles. This correlation function is sensitive to changes in surface height as a function of radial distance, r. It may be used to determine surface roughness, and in some cases the average lateral distance between mounds.

In a similar vein, the slope–slope correlation functions are defined by

$$G_{\mathrm{lss}}(r,\theta) = \langle M_x(r\mathbf{e_1},\theta)\mathbf{M_x}(\mathbf{0},\theta)\rangle, \tag{3}$$

and

$$G_{\mathrm{tss}}(r,\theta) = \langle M_y(r\mathbf{e_1},\theta)\mathbf{M_y}(\mathbf{0},\theta)\rangle, \tag{4}$$

where $\mathbf{e_1}$ is the unit Cartesian vector parallel to the x-axis. $M_\ell(\mathbf{r},\theta)$ denotes the surface slope as the height difference between adjacent lattice sites in the ℓ-direction ($\ell = x, y$). The slope M_x refers to the direction *parallel* to the displacement vector, $r\mathbf{e_1}$, while by equation (4) the slope M_y refers to the direction *perpendicular* to the displacement vector. These slope–slope correlation functions are sensitive to changes in the surface normal, restricted to the xy-plane, and therefore may be used to determine characteristic length scales for important features in directions parallel to the high-symmetry plane of the surface.

Correlation functions (2)–(4) can be used to estimate: (i) the surface roughness; (ii) the size of mounds; and, when there are two length scales present, (iii) the typical distance between defects in the superlattice of mounds. First, by use of equation (2), the surface roughness is computed via

$$w(\theta) = \sqrt{G(0,\theta)}. \tag{5}$$

Second, the average mound size or 'critical radius', $r_c(\theta)$, corresponds to the first zero of either $G_{\mathrm{hh}}(r,\theta)$ or $G_{\mathrm{lss}}(r,\theta)$ as a function of r, for fixed θ, depending on crystal symmetry. Specifically, if mounds have square symmetry, then equation (3) is the appropriate correlation function to determine $r_c(\theta)$ and the coarsening exponent n by equation (1*b*) [25]. In cases of other symmetries that admit only one macroscopic length scale, correlation function (2) is preferred for computing $r_c(\theta)$, for consistency with previous works (e.g. [16]). Third, the length scale of dislocations in the superlattice of (square) mounds can be computed as the distance r for which $G_{\mathrm{tss}}(r,\theta) = \frac{1}{2}G_{\mathrm{tss}}(0,\theta)$. A discussion of equations (3) and (4), as well as the role of multiple length scales in computing $r_c(\theta)$, can be found in [25].

Our choice of correlation functions in this paper has been mainly motivated by similar notions that permeate a large part of the literature. This choice better serves our present comparison purposes. Hence, the use of alternate statistical tools lies beyond the scope of this paper.

3. Models and kinetic processes

In this section, we outline the atomistic lattice-gas models that we use to study mound evolution.

3.1. Basic SOS model

A simple yet surprisingly accurate stochastic model of epitaxial growth is the SOS model [51]. By this model, atoms may arrange themselves in a SC crystal lattice, forming bonds with each of their nearest neighbors. Overhangs and bulk vacancies are forbidden. The crystal surface is represented by an array of height columns, which may change by a single atomic unit during every transition between distinct states in the configuration space as adsorbed atoms (adatoms) hop on the surface. Most transitions between nearby states follow Arrhenius rates. In the basic model, external deposition occurs at a rate F (measured in atoms per unit time, per lattice site).

We choose a particularly simple version of the SOS model where detachment from an island boundary is not allowed, and the only processes included are surface diffusion and edge diffusion. Surface diffusion is described by the diffusion constant $D = \nu_0 \exp(-E_S/k_\mathrm{B}T)$, where ν_0 is an attempt frequency, E_S is a surface bonding energy, k_B is Boltzmann's constant, and T is the substrate (absolute) temperature. Singly coordinated edge atoms are allowed to move along an island edge at a rate $D_e = D\exp(-E_N/k_\mathrm{B}T)$, where E_N can be interpreted as the bond strength of the in-plane bond between the edge atom and the island edge. There is no additional barrier for atoms to hop around a corner or around kinks (from a position with one nearest neighbor to a position with two or more nearest neighbors). For all results shown below, we choose dimensionless parameters such that $D/F = 10^6$, and $D_e/D = 0$ for the case of no edge diffusion, and $D_e/D = 0.01$ when we include edge diffusion. The value $D_e/D = 0.01$ is chosen empirically so that edge diffusion leads to compact islands.

3.2. Step-edge barrier

The SOS transition rates (section 3.1) may be modified to account for ES barriers at step edges. In this case, the energy $E_\pm$ can be added to E_S. In our notation, E_+ is the additional barrier that an adatom needs to overcome in order to move across the step edge from the upper terrace to the lower terrace (to attach to the step edge). This is shown schematically in figure 1. In principle, we could also include a (possibly negative) energy barrier, E_-, that is an additional barrier that needs to be overcome for attachment to a step edge from the lower terrace (not shown in figure 1). We will set $E_- = 0$ in an effort to use a minimal model that singles out the most important atomistic mechanism influencing mound evolution. Thus, the hopping rate for an adatom attaching to a step from above is $D' = D\exp(-E_+/k_\mathrm{B}T)$. The corresponding rate for an adatom attaching from below is $D'' = D\exp(-E_-/k_\mathrm{B}T)$ which simplifies to $D'' = D$.

3.3. Transient mobility

Transient mobility is one of the downward transport mechanism discussed in this paper. We adopt the SOS model presented in [16], which is one of only a few KMC prescriptions for TM. Similar models of a TM-like deposition process are described earlier [14, 53, 54]. TM is usually invoked for modeling growth that involves 'hot precursors'. The deposition process in [16], depicted in figure 3, has two stages: first, a lattice site is selected at random for deposition. Next, a local search within the square of side length $2R + 1$ about the initially chosen site is performed for the site that would give the deposited atom highest coordination number, n. If the search results in a unique maximum coordination number among the affected collection of sites, the deposited atom is placed at that site. In the event of a tie, the site closest to the initial site is selected. In this deposition process, R is a 'search radius' which is supposed to reflect the transient kinetic energy imparted to the atom by deposition and adsorption. We note that different precursors can have different kinetic energies, which would require different search radii R in the simulation. For simplicity we use just one value for R for all atoms which can be regarded as an average. For vicinal surfaces, TM may involve significant lateral mass transport without an uphill or downhill bias. For surfaces with mounds, on the other hand, regions between mounds have a high concentration of sites that would provide a deposited atom with two or more nearest neighbors, and therefore TM induces a downhill surface current.

Transient diffusion atoms, or 'hot precursors', received early attention as a candidate mechanism that could explain reflection high-energy electron diffraction (RHEED) oscillations observed in experiments of low-temperature metal-on-metal growth [1]. However, the inclusion of this mechanism in analytical and numerical studies has been mostly lacking. While TM has been addressed recently via a rate-equation approach [55, 56], KMC studies with TM are rare. Following the work by Einstein and others [55, 56], Amar and Semaan recently performed a study [57] of both superdiffusion and subdiffusion in the submonolayer regime. Still, it seems that the most comprehensive study of the impact of TM on mound growth, found in [16], is by now over twenty years old.

In [16], the authors show that TM can effectively oppose the ES barrier and lead to slope stabilization during growth by using the search procedure described above. The extent of their simulation data, however, is quite limited: only two parameter sets are used. In section 5, we enrich their study [16] by methodically examining the effects of ES barrier strength, expressed in terms of Arrhenius factor $D'/D = \exp(-E_+/k_\mathrm{B}T)$, and length R.

3.4. Downward funneling

Downward funneling is the other downward transport mechanism discussed in this paper. The energetic barriers and transition rates of the SOS model can be readily incorporated into more complicated geometries, e.g. BCC or face-centered cubic geometries. We will consider BCC crystal geometries in addition to the SC geometry of the SOS model in order to include DF in one of our atomistic models. Surface diffusion and edge diffusion of singly coordinated edge atoms are the processes that are allowed in the BCC geometry and they are described by D and D_e, respectively. As for the cubic symmetry, $D_e = D\exp(-E_N/k_BT)$, where E_N can again be interpreted as the bond strength of the in-plane bond between the edge atom and the island edge. There is no additional barrier for atoms to hop around a corner or around kinks.

Mimicking the SOS assumption in BCC geometry, the most basic prescription of DF avoids configurations involving overhangs and voids. This is achieved by asserting that any atom deposited to a site with three or fewer supporting atoms in a lower layer immediately relaxes to a site with *full support*, i.e. four supporting atoms in the next layer. A schematic of this DF process is shown in figure 2.

Alternate versions of DF have been proposed, including the restricted DF [13], a type of DF involving a certain probability of funneling upward [43, 44, 52], and the inclusion of low-barrier processes that favor downward transport [3]. Since each of these alternatives is expected to yield similar results, we utilize the above, simplest version of DF in this paper.

3.5. Validation

As described in sections 3.1–3.4, we have two different KMC models that use a cubic and a BCC geometry. Both codes have been validated extensively as follows: for both models, we have compared submonolayer results for the island densities, adatom densities, and island size distribution functions for different values of D/F to results that were previously published in the literature with other codes [61, 62]. We found excellent agreement for all these quantities (plots are not shown here). With the cubic SOS code we also reproduced the scaling exponents and island morphologies that were published in [16] for TM. Again, we obtained excellent agreement within the statistical accuracy of such codes. For the code with a BCC geometry, we have compared the morphology of mounds and scaling exponents for surface roughening and mound coarsening to the results of [12] and also find agreement. We are therefore confident that our implementation of the KMC models described is correct.

4. Results: qualitative description of mounding

In this section, we discuss qualitative features of mound growth observed in our simulations, and how these features change with certain model parameters which are associated with key atomistic processes. Specifically, we focus on the effect of (a) ES barrier strength (measured in terms of D'/D), (b) step-edge diffusion (measured in terms of edge diffusion rate D_e/D), and (c) type and strength of downward transport (including the case of no transport). In figures 4–6, we compare morphologies at $\theta = 1000$ monolayers of coverage as parameters relevant to cases (a)–(c) are varied.

4.1. ES barrier strength

For an initially flat surface, in the presence of material deposition on the surface from above, adatoms nucleate and form small islands. These islands may then grow until they reach a critical size, L_c, for which second-layer nucleation becomes likely. This process may then repeat for the second and subsequent layers, until an initial mound morphology is established. If there is no ES barrier, $E_+ = 0$, most atoms landing in the second layer are readily incorporated into a nearby island edge, often resulting in layer-by-layer growth. (Note that L_c is of the order of the typical island spacing which scales as $(D/F)^{1/6}$ for irreversible aggregation). On the other hand, if interlayer transport is inhibited, the probabililty of two or more adatoms being present on top of an island increases, thus resulting in more frequent second-layer nucleation events and smaller L_c (see [58] for further discussion on second-layer nucleation). Morphologies from KMC simulations are shown in figures 4 and 5. These results provide visual confirmation that the island size decreases with the ES barrier strength (which is taken to increase from the left to the right column in figures 4 and 5).

4.2. Step-edge diffusion

The parameter D_e (step-edge diffusion rate) most directly affects the shape of mounds, but may indirectly influence mound size. An example of the former effect can be seen in the fractile nature of islands in diffusion limited aggregation, when thermal detachment from islands and transport along island edges are neglected. Even if thermal detachment is suppressed, diffusion along island edges leads to compact islands. In the extreme case of very large edge diffusion rate D_e, islands quickly approach their equilibrium crystal shape as determined by their Wulff plot [59]. This feature of islands with sufficiently high edge diffusion can be seen in figure 4, which shows morphologies from KMC simulations that are completely irreversible (with no thermal detachment) but allow high edge diffusivity ($D_e/D = 0.01$). In most cases, mounds are nearly square. In contrast, when edge diffusion is turned off, mounds should retain some degree of irregularity. This effect is seen in figure 5, where thermal detachment and edge diffusion are both turned off.

One additional, indirect effect of edge diffusion is that it may enhance second-layer nucleation [60], and therefore contribute to smaller mounds. Comparing the corresponding panels in figures 4 and 5, for which all simulation parameters except edge diffusivity are the same, one can see that this claim is true for most cases by visual inspection. Deviating from this trend are the TM cases in the bottom row in each of figures 4 and 5. In regard to these simulation results, we believe that the effect of TM is more influential on mound

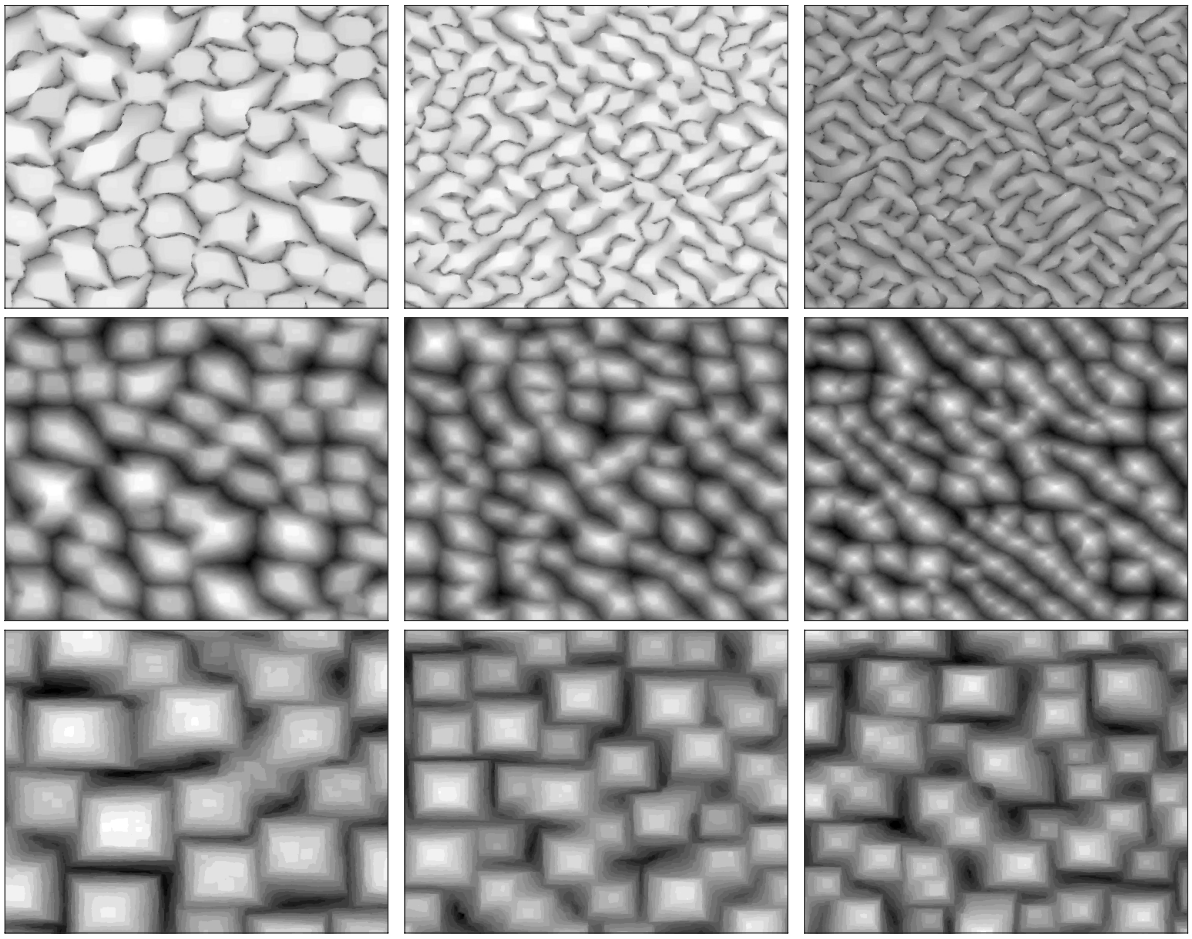

Figure 4. Surface morphologies from KMC simulations after 1000 monolayers of deposition when step-edge diffusion is included with $D_e/D = 0.01$. Top row: no downward transport is present. Middle row: DF is included. Bottom row: TM with $R = 3$. For all rows the strength of the step-edge (ES) barrier increases from left to right with $D'/D = 0.1$ (left column), $D'/D = 0.01$ (middle column), and $D'/D = 0$ (right column). Each panel represents a cross section of size 500×500 of the simulation lattice.

morphology than edge diffusion, e.g. islands are much more compact in the bottom row of figure 5 than in other cases. One might argue that TM with sufficiently large R mimics the effect of edge diffusion (see discussion in section 4.1).

4.3. Downward transport

Finally, we address the effect of type and strength of downward transport. We consider three different downward transport scenarios: no transport (deposited atoms land at the initially chosen deposition site for an SC crystal); transport in the presence of DF; and transport with TM. For simulations that include DF, the strength of downward transport is determined exclusively by the local geometry near a deposition site. In the presence of TM, we use the adjustable parameter R, which determines the search area. A large R can allow for a deposited atom to be incorporated into a lower layer several lattice sites away from the initially chosen deposition site. In fact, in the extreme case with $R \to \infty$, deposited adatoms will always reach an island edge, if one exists, so that the surface grows layer by layer even in the presence of an infinite ES barrier. For decreasing R, there is competition between uphill-current-inducing ES barriers and a downhill surface current associated with TM. This situation qualitatively mimics the case of DF, but we do not observe quantitative agreement. TM also contributes an uphill surface current when the local geometry allows this (e.g. see figure 3), whereas DF only allows for a downhill current.

Figures 4 and 5 demonstrate the abovementioned differences between different cases of transport: in both figures the top row includes no transport cases, the middle row shows the corresponding DF cases, and the bottom row includes TM with $R = 3$. Lastly, in figure 6, we see the effect of increasing R from zero (top left), which is the same as the case of no transport, to $R = 11$ (bottom right). In these plots, there is a transition from fractile-like islands to irregular mounds to square mounds. We observe that TM with large R not only approaches layer-by-layer growth but can also mimic high-edge diffusion since the island shapes are close to square (bottom row of figure 6).

5. Results: quantitative description of mounding

In this section, we present simulation results for the scaling exponents of equation (1). In particular, we show the dependence of these exponents on ES barrier strength (section 5.1)

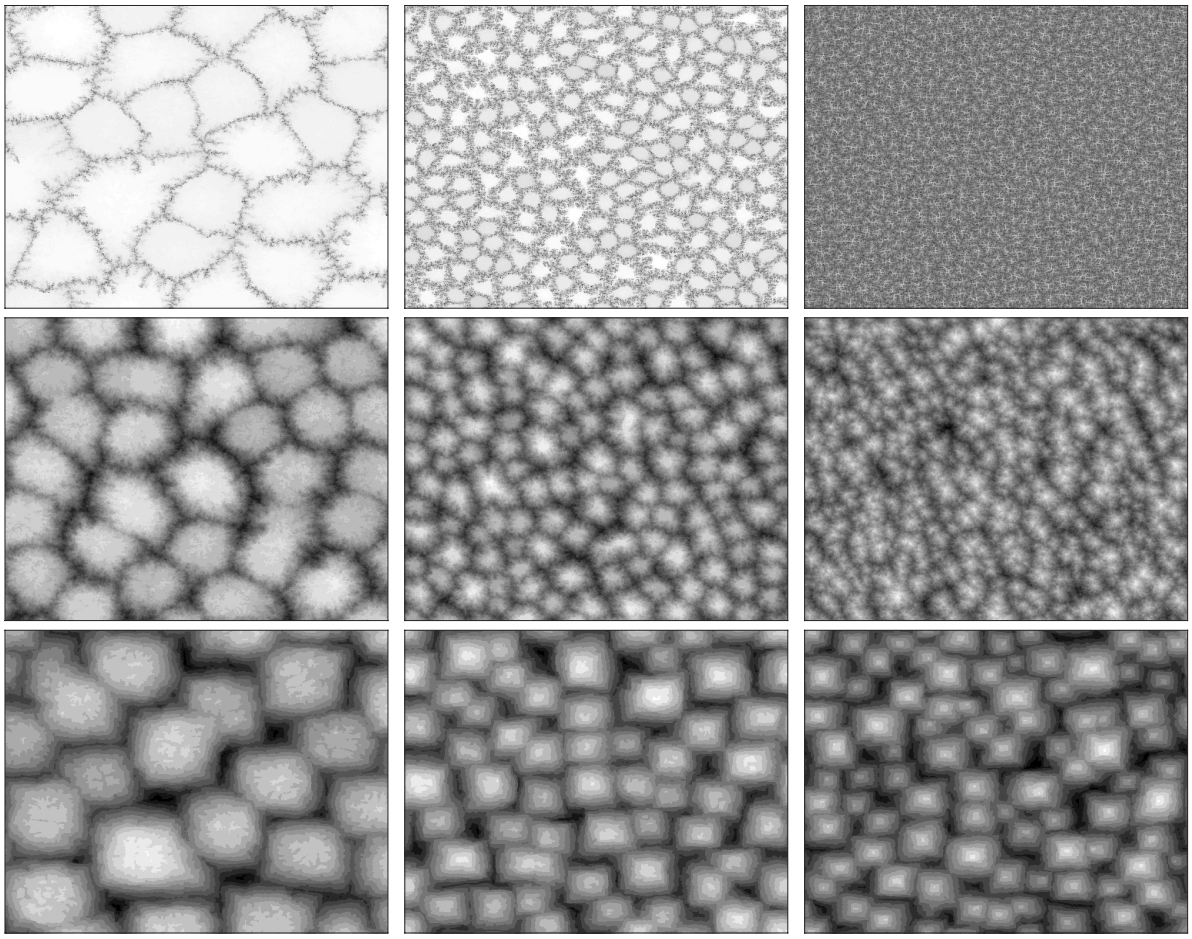

Figure 5. Surface morphologies from KMC simulations after 1000 monolayers of deposition without step edge diffusion, $D_e/D = 0$. Top row: no downward transport is present. Middle row: DF is included. Bottom row: TM with $R = 3$. For all rows the strength of the step-edge (ES) barrier increases from left to right with the values $D'/D = 0.1$ (left column), $D'/D = 0.01$ (middle column), and $D'/D = 0$ (right column). Each panel represents a cross section of size 500×500 of the simulation lattice.

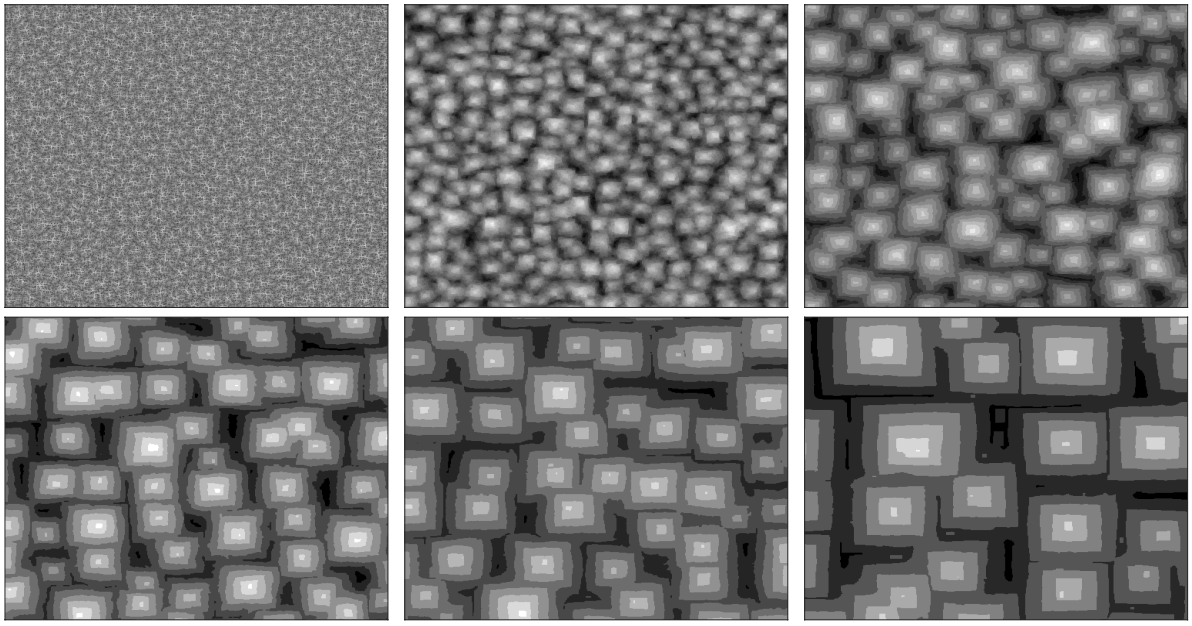

Figure 6. Surface morphologies from KMC simulations after 1000 monolayers of deposition when there is no diffusive interlayer transport (infinite ES barrier), no step edge diffusion, and TM is present. From left to right column: the respective values of R used are $R = 0, 1, 3$ (top row), and $R = 5, 7, 11$ (bottom row). Each panel represents a cross section of size 500×500 of the simulation lattice.

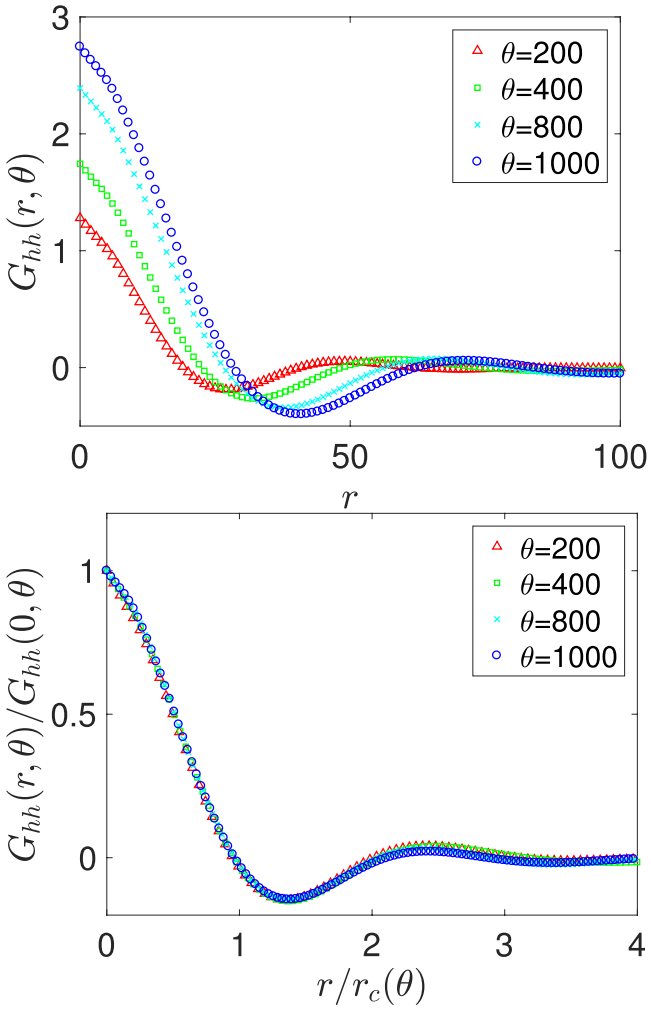

Figure 7. Plots of the height–height correlation function, $G_{\rm hh}(r,\theta)$, versus distance r (top panel), and the scaled version $G_{\rm hh}(r,\theta)/G_{\rm hh}(0,\theta)$ versus r/r_c (bottom panel) for KMC simulations with TM ($R=3$). The simulations include an infinite ES barrier ($D'/D=0$), and do not include edge diffusion.

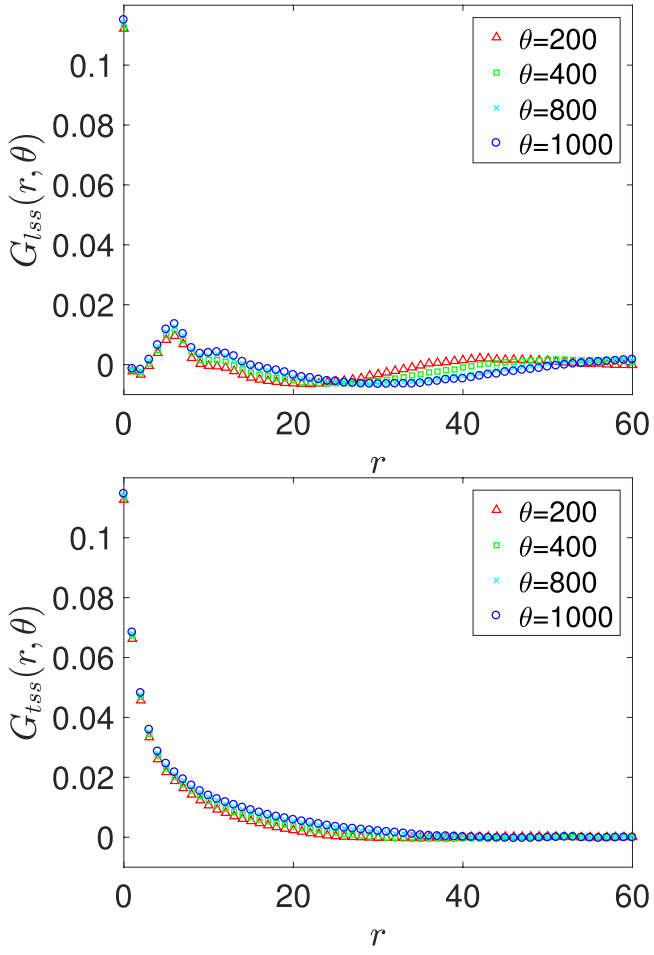

Figure 8. Plots of the slope–slope correlation functions, $G_{\rm lss}$ and $G_{\rm tss}$, versus distance r for KMC simulations with TM ($R=3$). Top panel: longitudinal slope–slope correlation function, $G_{\rm lss}(r,\theta)$, versus r/r_c; see equation (3). Bottom panel: transverse slope–slope correlation function, $G_{\rm tss}(r,\theta)$, versus r; see equation (4). The simulations include an infinite ES barrier ($D'/D=0$), and do not include edge diffusion. The discontinuity shown in the longitudinal correlation function (top panel) is likely due to the discrete nature of features when $r=1,2$.

and TM radius, i.e. the strength of a transient kinetic process related to deposition (section 5.2). In addition, we show how the island shape, controlled by the edge diffusivity, D_e, affects these dependencies (section 5.3).

All scaling exponents that we report here are computed using the surface correlation functions described in section 2.3. In each case, we carefully choose normalized correlation functions, expressed by $G(r,\theta)/G(0,\theta)$, that depend on coverage (time), θ, only through the average mound radius, $r_c(\theta)$. Specifically, $G(r,\theta)$ must satisfy the scaling ansatz

$$G(r,\theta) = f(r/r_c)G(0,\theta), \tag{6}$$

where $f(x)$ is an unknown scaling function, which is determined via numerical simulations. Figures 7 and 8 show examples of the correlation functions that we employ, as well as the collapse of their rescaled data points in accordance with (6). Note that $G(0,\theta) = w^2(r,\theta)$ if G is the height–height correlation function of equation (2).

To be more precise, the exponents β and n that we present in this section are obtained as follows. First, we plot the height–height correlation function, $G_{\rm hh}(r,\theta)$. If the data of the scaled form of this function suitably collapses (as shown in the bottom panel of figure 7), only one length scale is present. In this case, we obtain r_c from the first zero crossing of $G_{\rm hh}(r,\theta)$ and the respective roughness as defined in equation (5). However, when there is no data collapse for $G_{\rm hh}$, two length scales are present, namely, the average distance between mounds and the average distance between dislocations in the superlattice of (square) mounds. In the case of two scales, we need to use the first zero crossing of slope–slope correlation function $G_{\rm lss}(r,\theta)$, as shown, for example, in the top panel of figure 8. (Accordingly, in the following data for n, we specify whether we used $G_{\rm hh}(r,\theta)$ or $G_{\rm lss}(r,\theta)$ to obtain n.) Note that the first zero crossing of slope–slope correlation function $G_{\rm tss}(r,\theta)$ can in principle be used to extract the length scale of the dislocations. However, this length scale is comparable to the size of the simulation lattice; thus, any value that we would extract for this length scale is not very meaningful. Therefore, we do not pursue this task in this paper.

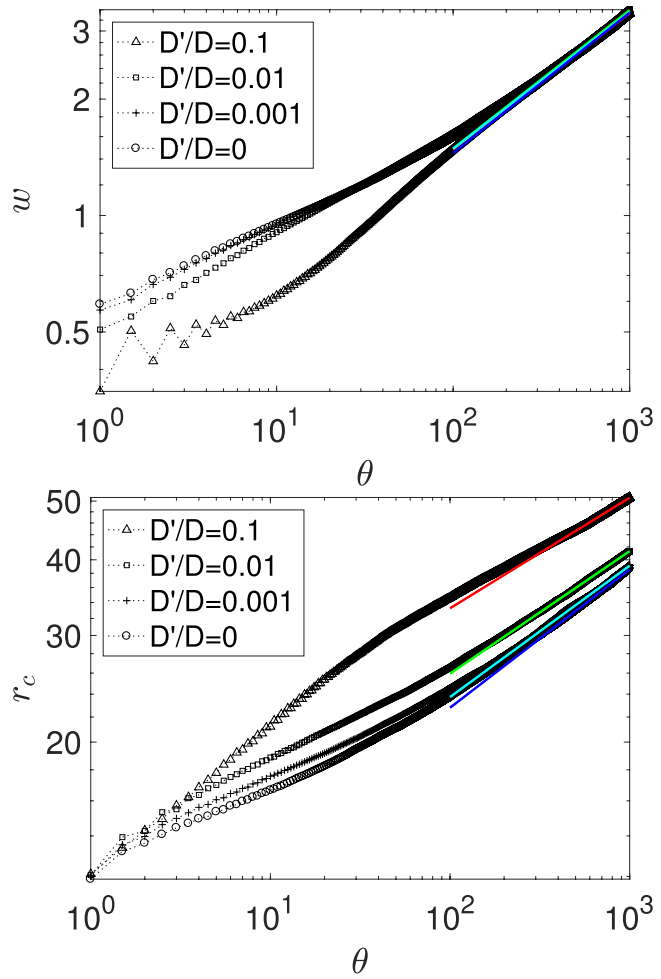

Figure 9. Log–log plots of the surface roughness (top panel) and mound radius (bottom panel) as a function of coverage, θ, for different values of the ES barrier. The data is computed from KMC simulations with TM ($R = 3$), with high edge diffusion ($D_e/D = 0.01$). The solid lines are a guide to the eye and correspond to the slope in the long-time regime.

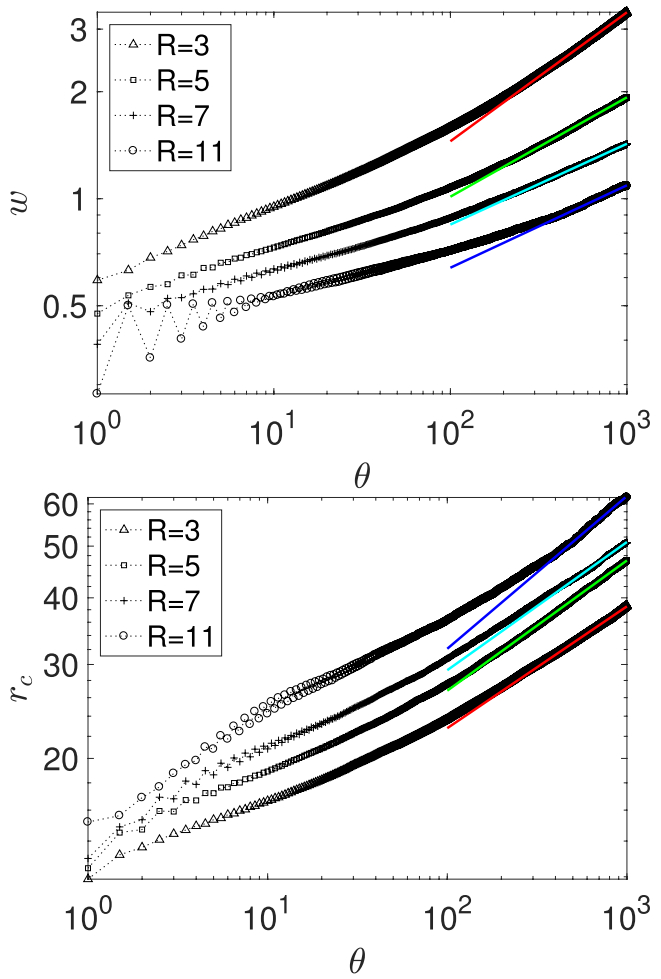

Figure 10. Log–log plots of the surface roughness (top panel) and mound radius (bottom panel) as a function of coverage, θ, for different values of the TM search area as defined by R. The data is computed from KMC simulations with TM, high edge diffusion with $D_e/D = 0.01$, and infinite ES barriers (no diffusive interlayer transport). The solid lines are a guide to the eye and correspond to the slope in the long-time regime.

Once the surface roughness and average mound radius are computed, we extract the exponents β and n of equation (1) in the long-time regime of our atomistic simulations. Specifically, β and n are the respective slopes of the lines fitted to data points $(\log\theta, \log w)$ and $(\log\theta, \log r_c)$, for sufficiently large θ. Figures 9 and 10 show typical regression lines used to measure these long-time scaling exponents for roughening and coarsening. In most cases, log–log plots such as those in figures 9 and 10 reveal approximately linear behavior in data between roughly 100 monolayers and 1000 monolayers of coverage.

In the remainder of this section, we summarize simulation results for exponents β and n for more than 40 parameter sets (see sections 5.1–5.3). In each case, our correlation functions result from averages over 4–10 independent KMC simulations on lattices of size either 1000×1000 or 500×500.

5.1. ES barrier dependence

Intuitively, one expects surfaces grown with large ES barriers to roughen faster than those with small (but nonzero) ES barriers. This behavior, discussed in section 4, is revealed by the data of table 1 which shows β and n as a function of the ES barrier strength. All other parameters are fixed; specifically, $D/F = 10^6$, detachment of atoms from step edges is forbidden, and hopping along island edges is efficient ($D_e/D = 0.01$). In the case of TM, we present results with different values for the search radius R. The case with $D'/D = 1$ is shown in table 1 as a reference case, but is not discussed since layer-by-layer growth is preferred over mounding when $D' = D$. The exponents reported in table 1 for DF are obtained from the slopes shown in figure 9.

Table 1. Scaling exponents β and n for the separate cases with DF and TM as a function of step edge barrier D'/D, with $D_e/D = 0.01$ and $R = 3$. In each case, exponents are based on the longitudinal slope–slope correlation function, $G_{\mathrm{lss}}(r, \theta)$ (equation (3)), except for TM when $D'/D = 10^{-1}$.

	DF		TM ($R = 3$)		TM ($R = 5$)		TM ($R = 7$)	
D'/D	β	n	β	n	β	n	β	n
10^{0}	0.53	0.21	0.57	0.25	0.38	0.24	0.27	0.24
10^{-1}	0.28	0.24	0.34	0.17	0.26	0.17	0.23	0.21
10^{-2}	0.29	0.29	0.34	0.20	0.26	0.22	0.22	0.22
10^{-3}	0.31	0.31	0.35	0.21	0.27	0.24	0.22	0.23
$10^{-\infty}$	0.36	0.33	0.36	0.23	0.28	0.25	0.22	0.23

Table 2. Scaling exponents β and n for TM as a function of R with $D'/D = 0$, and step edge diffusion with $D_e/D = 0.01$. In each case, exponents are based on the longitudinal slope–slope correlation function, $G_{\mathrm{lss}}(r, \theta)$ (equation (3)).

R	β	n
0	0.50	$\simeq$0
1	0.40	0.22
3	0.36	0.23
5	0.28	0.25
7	0.22	0.22
11	0.23	0.29

Table 1 shows an increase of β for DF as the barrier increases (D'/D decreases) from $\beta = 0.28$ for the smallest barrier to $\beta = 0.36$ for an infinite ES barrier. In the case with TM, β changes very little as a function of D'/D for all values of R (ignoring the case $D'/D = 1$). The coarsening exponent, n, increases with the ES barrier strength from $0.24 \simeq 1/4$ to $0.33 \simeq 1/3$ for DF. For TM, the coarsening exponent increases as well as D'/D decreases, and n changes from 0.17 to 0.23 for TM with $R = 3$, and from 0.17 to 0.25 for $R = 5$. The increase is a little less pronounced for $R = 7$, and n changes from 0.21 to 0.23. This increase of n is in contrast to results in [16] where a decrease of the coarsening exponent with increasing ES barrier was reported. We note that the experiments by Zuo and Wendelken [9] reported a coarsening exponent of $n = 0.25$ for Cu/Cu(0 0 1). This exponent agrees with our results for DF and moderate ES barriers with $D/D = 10^{-1}$, as well as our results for TM and larger ES barriers. DFT results of Yildirim and Rahman [63] suggest that the additional step edge barrier for Cu/Cu(0 0 1) is around 60 meV, which at the experimental temperature of [9] corresponds to a value of $D/D \simeq 10^{-1}$. We therefore speculate that for this system DF is the relevant mechanism for downward transport. On the other hand, the value $n = 0.16$ reported for Fe/Fe(0 0 1) [8] does not agree with any of our simulations.

The simultaneous increase of these exponents is related to slope selection. In the asymptotic (with time) scaling regime, β and n should be equal, which is true for several cases in table 1. In particular, in the case with DF we observe slope selection with exponents that increase continuously as a function of the step-edge barrier strength. This observation should be contrasted to previous results where usually only one value for the exponents was reported. In the case with TM and $R = 3, 5$, our results do not predict slope selection, while we predict slope selection for TM and $R = 7$. This dependence of slope selection on the search area R is discussed more in section 5.2. We note that it is also possible that in fact the values for both β and n for TM that are reported in table 1 will continue to change until they become equal, so that the average surface slope is stabilized in the asymptotic regime.

Table 3. Scaling exponents β and n for DF and TM as a function of the step edge barrier D'/D, with $D_e/D = 0$ and $R = 3$ (for the case with TM). In each case, exponents are based on the height–height correlation function, $G_{\mathrm{hh}}(r, \theta)$ (equation (2)).

	DF		TM ($R = 3$)	
D'/D	β	n	β	n
10^{0}	LBL		0.69	0.20
10^{-1}	0.29	0.13	0.29	0.13
10^{-2}	0.18	0.18	0.22	0.18
10^{-3}	0.18	0.23	0.21	0.21
$10^{-\infty}$	0.18	0.33	0.24	0.24

5.2. TM search area dependence

In the case with TM, recall that the parameter R defines the size of the search area for freshly deposited atoms. This R can be interpreted as a parameter that controls the strength or efficiency for downward transport. In addition, R can be viewed as a length that effectively increases surface diffusion and step edge diffusion in the simulations, as is discussed in more detail below.

It has been claimed that the exact value of R used in simulations has little or no effect on the scaling exponents [16]. Table 2 summarizes our results for scaling exponents β and n for different values of R in the presence of an infinite ES barrier ($D'/D = 0$) and step edge diffusion with $D_e/D = 0.01$. Clearly, by our simulations β decreases from 0.40 to 0.22 as R increases from 1 to 7. The exponent n also changes, but in a less systematic way. Specifically, n increases as R is varied from $R = 1$ to $R = 5$, and one might argue that n saturates for $R = 7$. We observe slope selection for $R = 7$, and arguably (within the accuracy of our method of extracting exponents) for $R = 5$. For larger values of R we do not observe slope selection.

We speculate that the following argument explains these results: when $R = 0$, there is no downward transport, and hence there is no slope selection. Small but finite values of R (e.g. $R = 1$ and $R = 3$) do not suffice to cause downward transport that would lead to slope selection on the timescale of our simulations, though it is possible that slope selection occurs for much larger coverages. One could say that the values $R = 1$ and $R = 3$ are too close to $R = 0$. Slope selection is only attained for intermediate values of R (in this case $R = 5$ and $R = 7$). On the other hand, in regard to large values of R, the value $R = 11$ corresponds to a very different case,

Table 4. Scaling exponents β and n in the case with TM as a function of R with $D'/D = 0$ and $D_e/D = 0$. When $R = 0$, 1, 3, exponents are based on the height–height correlation function, $G_{\rm hh}(r, \theta)$ (equation (2)). For $R \geqslant 5$, $G_{\rm lss}(r, \theta)$ (equation (3)) is used since the square symmetry of mounds is more emphatic; see figure 6.

R	β	n
0	0.50	$\simeq$0
1	0.23	0.18
3	0.24	0.24
5	0.22	0.25
7	0.21	0.26
11	0.22	0.27

and in fact we believe that this is not physically meaningful. For $R = 11$, the search area is of the order of the size of an island (or mound). Therefore, TM allows adatoms to attach to the other side of an island, and even to a different island. Large values of R effectively induce layer-by-layer growth (without mounds). This effect is also present when there is no step edge diffusion. We further discuss this effect in section 5.3.

5.3. Role of edge diffusion

In addition, we examine the effect of the step edge barrier and size of the search area, defined by R, during TM when there is no step edge diffusion ($D_e/D = 0$). The data in tables 3 and 4 reproduces the data in tables 1 and 2, respectively, yet without edge diffusion. Setting $D_e/D = 0$ here primarily affects surface roughness, which is higher than in the case with nonzero edge diffusion. While this claim seems counter-intuitive at first, it can actually be explained easily: when edge diffusion is present, the island shapes are more compact. As a result, the average distance from any site on top of an island to the closest step edge increases as edge diffusion increases. Hence, second-layer nucleation becomes more likely, and the system roughens faster.

As D'/D increases, the coarsening exponent, n, increases for both DF and TM. The computed values of n are close to the ones for the case with edge diffusion (see table 1). On the other hand, the behavior of the roughening exponent, β, is different. For both DF and TM, exponent β decreases when D'/D changes from $D'/D = 10^{-1}$ to 10^{-2}; but β is almost constant as D'/D decreases further. By our simulation results, we observe slope selection in a few cases, but not in all. We speculate that the exponents are still changing with time, or that the fractal nature of the island edges (that can clearly be seen for example in figures 5 and 6) affects the roughening and coarsening behavior (see below).

In regard to TM, in table 3 we show the dependence of exponents β and n on D'/D for $R = 3$. As R increases, the islands become more compact, as explained above. By comparing the data of tables 2 and 4 in the case with TM, we notice that for $R = 5$ and $R = 7$ the computed values of β and n are quite close, since the increased value of R mimics step edge diffusion. Without edge diffusion, we see in table 4 a behavior of the scaling exponents that is consistent with slope selection for $R = 3$ and $R = 5$. As R increases further, we find that $\beta - n < 0$, which means that slopes are actually decreasing without slope selection. We repeat that the value $R = 11$, or larger values of R, are not physically meaningful, because atoms that are deposited on the surface from above can attach to the other side on an island, or to other islands. In fact, as R increases further (and approaches the linear size of the simulation lattice), one tends to achieve perfect layer-by-layer growth, because there is always a preferred site in a lower layer until the layer is filled completely. This trend is evident in figure 6 for $R = 11$.

In regard to table 4, we do not observe slope selection for $R = 1$. In this case, island edges are quite rough and can be described as fractal-like. While we can certainly compute a value of the 'slope' according to our definition, we argue it is not physically clear what the slope is. Therefore, it is not surprising that 'slope selection' is not attained. Also, as we discuss in section 5.2, $R = 1$ might simply be too close to $R = 0$.

6. Discussion and conclusion

In this paper, we presented and discussed results of extensive KMC simulations that explore the dependence of the roughening and coarsening exponents, β and n, for mound formation on the underlying atomistic model parameters. Our main conclusions are: (i) the asymptotic scaling exponents do not just attain one universal value based on crystalline symmetry, but instead depend on details of atomistic processes; and (ii) effective scaling exponents measured in the long-time regime change continuously as a function of simulation parameters.

This behavior of our simulation results is best illustrated via the observed dependence of β and n as a function of the step edge barrier D'/D in the presence of edge diffusion. When DF is present in our KMC simulations, both exponents increase from 1/4 to 1/3 as the step edge barrier increases, and there is slope selection for all cases (see table 1). For TM in our simulations, n increases from 0.17 to 1/4 when $R = 3$ and $R = 5$, and there is no slope selection (table 1). To place these results in the context of some past works, note that continuum theories for coarsening of surfaces have predicted a scaling exponent of $n = 1/6$ if a 6th-order term is the highest-order term in the evolution equation for the surface height. In contrast, if the highest-order term in the evolution equation is of 4th order, the continuum prediction is $n = 1/4$. Intrigued by our simulation results, we speculate that under certain growth conditions both (4th- and 6th-order) terms are present in the appropriate continuum limit of the atomistic model. The step edge barrier plausibly controls the relative importance of each term, thus leading to a continuous transition of n from 1/6 to 1/4. Our results for the dependence of n on the size of the search area, R, suggest a similar, continuous transition from 1/6 to 1/4 (see tables 1, 2, and 4).

In the absence of edge diffusion, when $D_e/D = 0$, we reach similar conclusions. The corresponding data can be seen in tables 3 and 4, which demonstrate continuous changes of the scaling exponents β and n with model parameters. However,

in the case without edge diffusion, the results are more complicated because the island shape is altered significantly.

It is worthwhile to discuss the occurrence (when $\beta \simeq n$) or lack of slope selection in our simulations. As mentioned above, we do observe slope selection in some cases, but not in all cases. There are several possible reasons for the lack of slope selection in some cases. From a continuum (phenomenological) perspective, it is tempting to attribute this simulation result to the simultaneous presence of 4th- and 6th-order terms in an evolution equation for the surface height at the macroscale. The combination of these two terms may in turn result in effective exponents. The relative importance of these two terms might be different for the roughening and the coarsening exponent. Although this argument is appealing and interesting, it is incomplete since it is based on phenomenology.

Another possibility of explaining the lack of slope selection in some cases is that the corresponding simulations take place in an extended intermediate (long-time) regime, and have not yet reached the asymptotic regime required for slope selection. Although our simulations have reached coverages that are larger than those of previous works, we may not as yet rule out that we have not reached the asymptotic limit in all cases of physical interest. However, we note that all our exponents were obtained from log–log plots with (essentially) straight lines that extend over at least one decade. This gives us confidence that we either have reached the asymptotic regime, or that we are much closer to it than previous studies.

We also want to suggest a third possible reason for the lack of slope selection in some cases. As we discuss in sections 2 and 5, for simulations with square symmetries there are two length scales that are present: the length scale that is associated with the mound size (defined by r_c), and the length scale associated with the distance between dislocations in the superlattice of (square) mounds. As explained above, we always use the proper correlation function $G_{\rm hh}(r,\theta)$ or $G_{\rm lss}(r,\theta)$ when we measure n, and we are confident that n does indeed describe the scaling of the feature size. But we are not certain whether or not the roughness (and hence β) might be affected by the presence of a second length scale. We believe that the importance of the second length scale is indeed a subject that deserves further study.

Acknowledgments

The authors wish to thank Professor J W Evans for useful discussions. We acknowledge support from the National Science Foundation for this research. The research of JS and CR was supported by NSF Grant No. DMS-1412392. The research of DM was supported by NSF Grant No. DMS-1412769. The research of FG was supported by NSF Grant No. DMS-1412695.

ORCID iDs

Joshua P Schneider https://orcid.org/0000-0003-0143-2887
Dionisios Margetis https://orcid.org/0000-0001-9058-502X
Frederic Gibou https://orcid.org/0000-0001-7022-5262
Christian Ratsch https://orcid.org/0000-0001-5215-8385

References

[1] Egelhoff W Jr and Jacob I 1989 *Phys. Rev. Lett.* **62** 921
[2] Evans J W, Sanders D, Thiel P A and DePristo A E 1990 *Phys. Rev.* B **41** 5410
[3] Shim Y and Amar J G 2010 *Phys. Rev.* B **81** 045416
[4] Villain J 1991 *J. Phys.* I **1** 19 (1991)
[5] Ehrlich G and Hudda F 1966 *J. Chem. Phys.* **44** 1039
[6] Schwoebel R L and Shipsey E J 1966 *J. Appl. Phys.* **37** 3682
[7] Johnson M, Orme C, Hunt A, Graff D, Sudijono J, Sander L and Orr B 1994 *Phys. Rev. Lett.* **72** 116
[8] Stroscio J A, Pierce D, Stiles M, Zangwill A and Sander L 1995 *Phys. Rev. Lett.* **75** 4246
[9] Zuo J-K and Wendelken J 1997 *Phys. Rev. Lett.* **78** 2791
[10] Caspersen K, Layson A R, Stoldt C, Fournee V, Thiel P A and Evans J W 2002 *Phys. Rev.* B **65** 193407
[11] Evans J 1991 *Phys. Rev.* B **43** 3897
[12] Amar J G and Family F 1996 *Phys. Rev.* B **54** 14742
[13] Caspersen K and Evans J 2001 *Phys. Rev.* B **64** 075401
[14] Clarke S and Vvedensky D D 1988 *Phys. Rev.* B **37** 6559
[15] Šmilauer P, Wilby M R and Vvedensky D D 1993 *Phys. Rev.* B **47** 4119
[16] Šmilauer P and Vvedensky D D 1995 *Phys. Rev.* B **52** 14263
[17] Evans J, Thiel P and Bartelt M C 2006 *Surf. Sci. Rep.* **61** 1
[18] Michely T and Krug J 2012 *Islands, Mounds and Atoms* vol 42 (Berlin: Springer)
[19] Siegert M and Plischke M 1994 *Phys. Rev. Lett.* **73** 1517
[20] Hunt A, Orme C, Williams D, Orr B and Sander L 1994 *Europhys. Lett.* **27** 611
[21] Siegert M 1997 *Physica* A **239** 420
[22] Siegert M, Plischke M and Zia R K 1997 *Phys. Rev. Lett.* **78** 3705
[23] Rost M and Krug J 1997 *Phys. Rev.* E **55** 3952
[24] Golubović L 1997 *Phys. Rev. Lett.* **78** 90
[25] Moldovan D and Golubovic L 2000 *Phys. Rev.* E **61** 6190
[26] Politi P and Torcini A 2000 *J. Phys. A: Math. Gen.* **33** L77
[27] Golubović L, Levandovsky A and Moldovan D 2002 *Phys. Rev. Lett.* **89** 266104
[28] Lo T S and Kohn R V 2002 *Physica* D **161** 237
[29] Politi P and Torcini A 2006 *Eur. Phys. J.* B **53** 401
[30] Biagi S, Misbah C and Politi P 2012 *Phys. Rev. Lett.* **109** 096101
[31] Biagi S, Misbah C and Politi P 2014 *Phys. Rev.* E **89** 062114
[32] Amar J G and Family F 1996 *Phys. Rev. Lett.* **77** 4584
[33] Amar J G 1999 *Phys. Rev.* B **60** R11317
[34] Bartelt M and Evans J W 1995 *Phys. Rev. Lett.* **75** 4250
[35] Šmilauer P, Rost M and Krug J 1999 *Phys. Rev.* E **59** R6263
[36] Siegert M and Plischke M 1996 *Phys. Rev.* E **53** 307
[37] Siegert M 1998 *Phys. Rev. Lett.* **81** 5481
[38] Bartelt M and Evans J 1999 *Surf. Sci.* **423** 189
[39] Shim Y and Amar J G 2006 *Phys. Rev.* B **73** 035423
[40] Ernst H-J, Fabre F, Folkerts R and Lapujoulade J 1994 *Phys. Rev. Lett.* **72** 112
[41] Elliott W, Miceli P F, Tse T and Stephens P 1996 *Phys. Rev.* B **54** 17938
[42] Stoldt C, Caspersen K, Bartelt M, Jenks C J, Evans J W and Thiel P A 2000 *Phys. Rev. Lett.* **85** 800
[43] Yu J and Amar J G 2002 *Phys. Rev. Lett.* **89** 286103
[44] Yu J and Amar J G 2004 *Phys. Rev.* B **69** 045426
[45] Borovikov V and Amar J G 2005 *Phys. Rev.* B **72** 085460
[46] Mullins W W 1957 *J. Appl. Phys.* **28** 333
[47] Bray A 1994 *Adv. Phys.* **43** 357
[48] Lifshitz I M and Slyozov V V 1961 *J. Phys. Chem. Solids* **19** 35
[49] Wagner C 1961 *Z. Electrochem.* **65** 581
[50] Golubović L, Levandovsky A and Moldovan D 2011 *East Asian J. Appl. Math.* **1** 297

[51] Weeks J D and Gilmer G H 1979 *Adv. Chem. Phys.* **40** 157
[52] Yu J and Amar J G 2002 *Phys. Rev.* E **66** 021603
[53] Clarke S and Vvedensky D D 1988 *J. Appl. Phys.* **63** 2272
[54] Wolf D and Villain J 1990 *Europhys. Lett.* **13** 389
[55] Morales-Cifuentes J R, Einstein T and Pimpinelli A 2014 *Phys. Rev. Lett.* **113** 246101
[56] Einstein T L, Pimpinelli A, González D L and Morales-Cifuentes J R 2015 *J. Phys.: Conf. Ser.* **640** 012024
[57] Amar J G and Semaan M 2016 *Phys. Rev.* E **93** 062805
[58] Krug J 2000 *Eur. Phys. J.* B **18** 713
[59] Rottman C and Wortis M 1984 *Phys. Rep.* **103** 59
[60] Ratsch C, Wheeler M and Gyure M 2000 *Phys. Rev.* B **62** 12636
[61] Ratsch C, Šmilauer P, Zangwill A and Vvendensky D D 1995 *Surf. Sci.* **329** L599
[62] Ratsch C, Gyure M F, Caflisch R E, Gibou F, Petersen M, Kang M, Garcia J and Vvedensky D D 2002 *Phys. Rev.* B **65** 19503
[63] Yildirim H and Rahman T S 2009 *Phys. Rev.* B **80** 235413